Substantially positive contributions of new particle formation to Cloud Condensation Nuclei under low supersaturation in China based on numerical model improvements

Chupeng Zhang[1#], Shangfei Hai[2,11#], Yang Gao[1*], Yuhang Wang[3*], Shaoqing Zhang[4,2], Lifang Sheng[2], Bin Zhao[5], Shuxiao Wang[5], Jingkun Jiang[5], Xin Huang[6], Shen Xiaojing[7], Sun Junying[7], Aura Lupascu[8],Manish Shrivastava[9], Jerome D. Fast[9], Wenxuan Cheng[1], Xiuwen Guo[1], Ming Chu[1], Nan Ma[10], Juan Hong[10], Qiaoqiao Wang[10], Xiaohong Yao[1] and Huiwang Gao[1]

[1]Frontiers Science Center for Deep Ocean Multispheres and Earth System, and Key Laboratory of Marine Environmental Science and Ecology, Ministry of Education, Ocean University of China, and Laoshan Laboratory, Qingdao, 266100, China

[2]College of Oceanic and Atmospheric Sciences, Ocean University of China, Qingdao, 266100, China

[3]School of Earth and Atmospheric Sciences, Georgia Institute of Technology, Atlanta, GA, 30332, USA

[4]Frontiers Science Center for Deep Ocean Multispheres and Earth System, and Key Laboratory of Physical Oceanography, Ocean University of China, and Laoshan Laboratory, Qingdao, 266100, China

[5]State Key Joint Laboratory of Environment Simulation and Pollution Control, School of Environment, Tsinghua University, Beijing, 100084 China,and State Environmental Protection Key Laboratory of Sources and Control of Air Pollution Complex, Beijing 100084, China

[6]School of Atmospheric Sciences, Nanjing University, Nanjing, 210023, China

[7]State Key Laboratory of Severe Weather & Key Laboratory of Atmospheric Chemistry of CMA, Chinese Academy of Meteorological Sciences, Beijing, 100081, China

[8]Institute for Advanced Sustainability Studies, Potsdam D-14467, Germany

[9]Atmospheric Sciences and Global Change Division, Pacific Northwest National Laboratory, Richland, WA, 99354, USA

[10]Institute for Environmental and Climate Research, Jinan University, Guangzhou, 510000, China

[11]CMA Earth System Modeling and Prediction Center, China Meteorological Administration, Beijing 100081, China

[#]Authors contributed equally to this study.

[*]To whom correspondence to: yanggao@ouc.edu.cn,
yuhang.wang@eas.gatech.eduyuhang.wang@eas.gatech.edu

Abstract

New particle formation (NPF) and subsequent particle growth are important sources of condensation nuclei (CN) and cloud condensation nuclei (CCN). While many observations have shown positive contributions of NPF to CCN at low supersaturation, negative NPF contributions were often simulated in polluted ~~environment~~environments. Using the observations in a ~~typical~~ coastal city of Qingdao, Beijing and Gucheng in North China, we thoroughly evaluate the simulated number concentrations of CN and CCN using a NPF-explicit parameterization embedded in WRF-Chem model. ~~In terms of~~For CN, the initial simulation shows large biases of particle number concentrations at 10–40 nm ~~(CN_{10-40})~~ and 40–100 nm ~~(CN_{40-100}).~~. By adjusting the process of gas-particle partitioning, including the mass accommodation coefficient of sulfuric acid, the phase changes of primary organic aerosol emissions and the condensational amount of nitric acid, the ~~concomitant~~ improvement of the particle growth process yields a ~~substantial reduction of~~substantially reduced overestimates of ~~CN_{10-40} and CN_{40-100}~~CN. Regarding CCN, SOA formed from the oxidation of semi-volatile and intermediate volatility organic vapors (SI-SOA) yield is an important contributor. ~~In~~At default settings, the ~~original WRF-Chem model with 20 size bins setting, the yield of~~ SI-SOA yield is too high without considering the differences in precursor oxidation rates ~~of the precursors.~~. Lowering the SI-SOA yield under linear-H_2SO_4 nucleation scheme results in much improved CCN simulations ~~of the observed CCN concentrations.~~compared to observations. On the basis of the bias-corrected model, we find ~~substantial~~substantially positive contributions of NPF to CCN at low supersaturation (~0.2%) ~~in Qingdao and~~ over the broad areas of China, primarily due to ~~the~~ competing effects of increasing particle hygroscopicity, a result of reductions in SI-SOA amount, surpassing that of particle size ~~decrease~~decreases. The bias-corrected model is robustly applicable to other schemes, such as quadratic-H_2SO_4 nucleation scheme, in terms of CN and CCN, though the dependence of CCN on SI-SOA yield is diminished likely due to changes in particle composition. This study highlights the potentially much larger NPF contributions to CCN on a regional and even global basis.

1. Introduction

New particle formation (NPF) is a process in which gaseous vapors nucleate and form critical molecular clusters, followed by subsequent growth to larger sizes through condensation and coagulation ~~(Kulmala et al., 2004; Kulmala et al., 2013; Lee et al., 2019)~~(Kulmala et al., 2004; Kulmala et al., 2013; Lee et al., 2019). Newly formed particles could effectively grow into the size of cloud condensation nuclei (CCN) under certain supersaturation (SS), which exerts an impact on the cloud microphysical process and global radiation balance ~~(Merikanto et al., 2009; Gordon et al., 2017; Kerminen et al., 2018; Ren et al., 2021)~~(Merikanto et al., 2009; Gordon et al., 2017; Kerminen et al., 2018; Ren et al., 2021). In addition, the efficient nucleation and explosive growth of particles may contribute to the formation of haze ~~(Guo et al., 2014)~~(Guo et al., 2014), affecting air quality and human health ~~(Yuan et al., 2015; Chu et al., 2019; Kulmala et al., 2021)~~(Yuan et al., 2015; Chu et al., 2019; Kulmala et al., 2021).

The overestimate of condensation nuclei (CN) in numerical models ~~are~~is commonly seen, despite the attempt to rectify the bias ~~(Matsui et al., 2013; Arghavani et al., 2022)~~(Matsui et al., 2013; Arghavani et al., 2022). It is a common way to reduce the nucleation rate which may reduce the particle number concentration in proportion ~~(Matsui et al., 2013)~~(Matsui et al., 2013). For instance, in the study of NPF in East Asia in the spring of 2009, even after lowering the nucleation rate in a regional model of WRF-Chem applied in their study, the reduced number concentration of particles at 10–130 nm remained to be overestimated ~~(Matsui et al., 2013).~~(Matsui et al., 2013). Using the same regional model and a similar method to reduce the nucleation rate, ~~Arghavani et al. (2022)~~Arghavani et al. (2022) found particle number concentration at 10–100 nm was still overestimated by nearly one order of magnitude, despite the effectiveness to

reduce the overestimates for the smaller particles such as 2.5–10 nm. In addition to the rate of NPF, the growth process of particles also has a crucial effect on particle number concentration and size distribution. In this process, the condensation of some chemical species such as sulfuric acid, nitrate and organic gases on particles plays a major role in particle growth ~~(Yao et al., 2018; Lee et al., 2019; Li et al., 2022)~~(Yao et al., 2018; Lee et al., 2019; Li et al., 2022), and the uncertainty of their condensation amount may lead to the bias of CN simulation.

In addition to CN, there are large discrepancies in the predicted CCN between the numerical models and observational results. Furthermore, as an important source of CCN ~~(Merikanto et al., 2009)~~(Merikanto et al., 2009), the contribution of nucleation to CCN quantified by numerical models is also highly uncertain. For example, in terms of predicting CCN, ~~Fanourgakis et al. (2019)~~Fanourgakis et al. (2019) evaluated the CCN concentrations simulated by 16 global aerosol–climate and chemistry transport models with observations at 9 sites in Europe and Japan from 2011 to 2015, and found that all models underestimated CCN concentrations with a mean normalized mean bias of -36% at low supersaturation (SS=0.2%). WRF-Chem models also tend to underestimate the contribution of NPF on CCN, especially at low supersaturation. The continuous observation of CCN concentrations throughout the year (July 2008–June 2009) carried out in Hyytiälä, Finland, showed that under low SS, nucleation enhanced the CCN by 106% and 110% at SS=0.1% and 0.2% respectively ~~(Sihto et al., 2011)~~(Sihto et al., 2011). Observations acquired in Beijing from July 12 to September 25, 2008, also suggested that nucleation significantly increases CCN at all supersaturations, even when supersaturation is low (i.e., 0.07% and 0.26%). Thus, the occurrence of NPF enhanced CCN by a factor of 1.7 and 2.2, respectively ~~(Yue et al., 2011)~~(Yue et al., 2011).

~~However, previous numerical experiments behave oppositely. For instance, Matsui et al. (2011) quantified the contribution of nucleation to CCN using WRF-chem in Beijing in August and September 2006 and found reduced CCN under low SS, e.g., when SS=0.02%, the concentration of CCN is reduced by up to ~50%. They attributed this to the fact that the small particles produced by nucleation may inhibit the growth~~

161 of the preexisting particles (Matsui et al., 2011). Similarly, Dong et al. (2019) conducted
162 NPF simulations with the WRF-Chem for the summer of 2008 focusing on the Midwest
163 of the United States, and found that the nucleation resulted in decreased CCN at low
164 supersaturation (SS=0.1%). Besides, a study carried out for East Asia in 2009 also
165 indicated that at low supersaturation (e.g. SS=0.1%), nucleation has little impact on
166 CCN (Matsui et al., 2013). The contrasting effects of nucleation on CCN at low
167 supersaturations in model and observations is not explained in these previous studies.
168   At the stage of particle growth, secondary organic aerosol (SOA) formed by
169 atmospheric oxidation of organic vapors is a major contributor to particle growth to
170 CCN-related sizes However, previous numerical experiments behave oppositely. For
171 instance, Matsui et al. (2011) quantified the contribution of nucleation to CCN using
172 WRF-chem in Beijing in August and September 2006 and found reduced CCN under
173 low SS, e.g., when SS=0.02%, the concentration of CCN is reduced by up to ~50%.
174 They attributed this to the fact that the small particles produced by nucleation may
175 inhibit the growth of the preexisting particles (Matsui et al., 2011). Similarly, Dong et
176 al. (2019) conducted NPF simulations with the WRF-Chem for the summer of 2008
177 focusing on the Midwest of the United States, and found that the nucleation resulted in
178 decreased CCN at low supersaturation (SS=0.1%). Besides, a study carried out for East
179 Asia in 2009 also indicated that at low supersaturation (e.g. SS=0.1%), nucleation has
180 little impact on CCN (Matsui et al., 2013). The contrasting effects of nucleation on CCN
181 at low supersaturations in model and observations is not explained in these previous
182 studies.
183   At the stage of particle growth, secondary organic aerosol (SOA) formed by
184 atmospheric oxidation of organic vapors is a major contributor to particle growth to
185 CCN-related sizes (Liu and Matsui, 2022; Qiao et al., 2021)(Liu and Matsui, 2022;
186 Qiao et al., 2021). SOA formed by multi-generational gas-phase oxidation of semi-
187 volatile and intermediate volatility organic compounds (S/IVOC) is called SI-SOA
188 (Jimenez et al., 2009; Zhang et al., 2007)(Jimenez et al., 2009; Zhang et al., 2007). Zhao
189 et al. (2016). Zhao et al. (2016) made a comprehensive assessment of the roles of
190 various SOA precursors in SOA formation in real atmosphere in China in 2010, and the

results demonstrated that evaporated POA and IVOC (i.e. S/IVOC) made a significant contribution to SOA, contributing up to 82% to the average SOA concentration in eastern China. However, the effect of SI-SOA on CCN has not been fully studied.

In this paper, WRF-Chem was applied to simulate the effect of the NPF on CCN in ~~Qingdao~~China in February 2017. The simulated results from the WRF-Chem model are firstly compared with observations in Qingdao, Beijing and Gucheng, exhibiting large biases in CN. This is followed by an improvement through a few processes. At the end, the impact of SI-SOA yield and nucleation on CCN is investigated.

2. Data and methods

2.1 Observations

The measurements used in this study were carried out over the sampling site from February 5 to 24, 2017 at the campus of Ocean University of China (36°09′37″N, 120°29′44″E~~-~~) in Qingdao, which is surrounded by residential buildings and is situated about 10 km away from the city center. A fast mobility particle sizer (FMPS, TSI Model 3091) was applied to measure the aerosol particle size distribution for the size range of 5.6 nm to 560 nm ~~(Liu et al., 2014b)~~(Liu et al., 2014b). The bulk CCN concentration is measured by a cloud condensation nuclei counter at three different supersaturations (0.2%, 0.4% and 0.6%) and each supersaturation lasts for 20 minutes. More information about the CCN measurement can be found in ~~Li et al. (2015)~~Li et al. (2015). The urban site in Beijing is located on the roof of the building of the Chinese Academy of Meteorological Sciences (CAMS, 39°95′N, 116°33′E) in the campus of the China Meteorological Administration, close to the main road with heavy traffic. The rural site is Gucheng (GC, 39°08′N, 115°40′E), located in Hebei Province, surrounded by farmland, and is a representative station of the severity of air pollution in Beijing Tianjin Hebei region. The particle number size distribution of these two sites in the range of 4–850 nm is measured by a Tandem Scanning Mobility Particle Sizer (TSMPS), and more information about the instruments can be found in ~~Shen et al. (2018)~~Shen et al. (2018).

2.2 Model configurations

WRF-Chem version 3.9 is used to simulate NPF events, with the main physical and chemical parameterization settings summarized in Table 1. The spatial resolution

221 is 36 km by 36 km with 35 vertical layers and a model top at 50 hPa. The regional

222 model simulations at a higher spatial resolution may be desirable in future when urban

223 pollution is focused. A continuous run from February 1 to 25, 2017, was conducted,

224 with the first five-day results as the spin-up and discarded in the analysis.

225 Table 1 WRF-Chem model configurations used in this work

	Model configuration
Microphysics	~~Morrison 2-moment microphysics scheme (Morrison et al., 2009)~~Morrison 2-moment microphysics scheme (Morrison et al., 2009)
Planetary Boundary Layer (PBL)	~~YSU boundary layer scheme (Hong et al., 2006)~~YSU boundary layer scheme (Hong et al., 2006)
Longwave and Shortwave Radiation	RRTMG longwave and shortwave radiation ~~(Iacono et al., 2008)~~(Iacono et al., 2008)
Land model	~~Unified Noah Land Surface scheme (Chen and Dudhia, 2000; Tewari et al., 2016)~~Unified Noah Land Surface scheme (Chen and Dudhia, 2000; Tewari et al., 2016)
Cumulus	~~Grell-3D cumulus parameterization scheme (Grell, 1993)~~Grell-3D cumulus parameterization scheme (Grell, 1993)
Aerosol module	MOSAIC module ~~(Zaveri et al., 2008; Matsui et al., 2011)~~(Zaveri et al., 2008; Matsui et al., 2011)
Gas-phase Chemistry	~~SAPRC-99 gas-phase chemistry scheme (Carter, 2000)~~SAPRC-99 gas-phase chemistry scheme (Carter, 2000)

226

227 The meteorological initial and boundary conditions are driven by Climate Forecast

228 System model version 2 (CFSv2; ~~(Saha et al., 2014)~~(Saha et al., 2014)) reanalysis

229 developed by National Centre for Environmental Prediction (NCEP). The initial and

230 boundary chemical conditions of WRF-Chem are provided by Community Atmosphere

231 Model with Chemistry (CAM-Chem; ~~(Buchholz et al., 2019)~~(Buchholz et al., 2019)).

Anthropogenic emissions for the year of 2017 are obtained from the Multiresolution Emission Inventory for China (MEIC, ~~http://www.meicmodel.org/~~http://www.meicmodel.org/) emission dataset ~~(Li et al., 2017; Zheng et al., 2018)~~(Li et al., 2017; Zheng et al., 2018).

The Model for Simulating Aerosol Interactions and Chemistry (MOSAIC) was used to delineate dynamic gas-particle mass transfer to represent the condensation growth of aerosol ~~(Zaveri et al., 2008)~~(Zaveri et al., 2008). The gas-particle partitioning of gas species on particles is regulated by the mass transfer rate, which is related to mass accommodation coefficient (α), a parameter involved in the model representing the probability of gas molecules entering the bulk liquid phase ~~(Pöschl et al., 1998)~~(Pöschl et al., 1998). The original setting of α for all condensing species for all size bins a in MOSAIC is 0.1 ~~(Zaveri et al., 2008)~~(Zaveri et al., 2008). In the default release of WRF-Chem, MOSAIC was implemented in the sectional framework with aerosol size distributions divided into 4 or 8 size bins spanning 39 nm to 10 µm in diameter. To explicitly express the nucleation and the growth of newly formed particles, the aerosol size range in the MOSAIC module was extended from 1 nm to 10 µm, with the number of aerosol size bins increased to 20 ~~(Matsui et al., 2011; Matsui et al., 2013; Lupascu et al., 2015; Lai et al., 2022)~~(Matsui et al., 2011; Matsui et al., 2013; Lupascu et al., 2015; Lai et al., 2022). The calculation method of CCN concentration in the WRF-chem model is referred to the study of ~~Matsui et al. (2011)~~Matsui et al. (2011). Based on Köhler theory, CCN concentrations under the three given supersaturations of 0.2%, 0.4% and 0.6% were calculated. The critical supersaturation (S_c) of each size bin in the WRF-chem model was calculated by the following formula:

$$S_c = \sqrt{\frac{4 \times a^3}{27 \times r^3 \times \kappa}} \tag{1}$$

$$a = \frac{2 \times \sigma}{R_v \times T \times \rho_\omega} \tag{2}$$

Where α (m) is the coefficient of the Kelvin effect, κ is the volume−averaged hygroscopicity, calculated using these values in Table 1, r (m) is the dry diameter, σ is droplet surface tension over water (0.076 N m^{-1}), R_v is the gas constant for water vapor

(461.6 J K^{-1}kg^{-1}), T (K) is the air temperature, and ρ_ω is the density of water (1000 kg m^{-3}).

Table 2 Hygroscopicity Parameters (κ) in the WRF-Chem Model

Species	Hygroscopicity (κ)
Sulfate	0.5
Ammonium	0.5
Nitrate	0.5
Black carbon	10^{-6}
Primary organic aerosol	0.14
Other inorganics	0.14
Sodium	1.16
Chloride	1.16

The chemical aging process of organic aerosols (OA) is modeled by the volatility basis set (VBS) approach, which was widely used in air quality models to represent complex mixtures of thousands of organic species ~~(Donahue et al., 2006; Shrivastava et al., 2011; Chrit et al., 2018)~~(Donahue et al., 2006; Shrivastava et al., 2011; Chrit et al., 2018). The VBS method classifies compounds according to the effective saturation concentration (c^*), which represents the proportion of the component in the gas phase to the particle phase ~~(Donahue et al., 2006)~~(Donahue et al., 2006), and species with higher c^* values are more volatile. The oxidation of highly volatile precursors to form relatively low volatile components represents the aging process of OA. OA consists of directly emitted primary organic aerosols and photochemically produced secondary organic aerosols (SOA) ~~(Shrivastava et al., 2011)~~(Shrivastava et al., 2011). In this study, the simplified 2-species VBS mechanism was applied to the simulation of SOA, during which primary organic aerosol was represented by two species based on volatility with effective saturation concentration c^* values (at 298 K and 1 atm) of 10^{-2} and 10^5 µg

281 m^{-3} ~~(Shrivastava et al., 2011)~~(Shrivastava et al., 2011). Primary organic aerosols with

282 c* of 10^5 µg m^{-3} refers to S/IVOC, which is in the gas phase under most atmospheric

283 conditions due to its high volatility, while for those primary organic matters with c* of

284 10^{-2} µg m^{-3}, is treated as gas phase as well in the original model. The SOA formed by

285 photochemical oxidation of S/IVOC precursors is called SI-SOA and the SOA formed

286 by oxidation of VOC precursors is named V-SOA. In the simplified 2-species VBS

287 mechanism, SI-SOA (c* of 10^{-2}µg m^{-3}) is formed by the oxidation reaction of S/IVOC

288 precursors (c* of 10^5µg m^{-3}) and OH with an oxidation rate constant of 4×10^{-11} cm^3

289 molec^{-1} s^{-1}. The equations for controlling the oxidation of S/IVOC precursors are as

290 follows:

291
$$POA(g)_{e,c} + OH \rightarrow SI - SOA(g)_{e,c} + 0.15SI - SOA(g)_{e,o} \qquad (3)$$

292
$$POA(g)_{e,o} + OH \rightarrow SI - SOA(g)_{e,o} + OH \qquad (4)$$
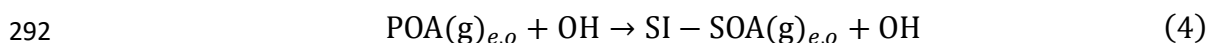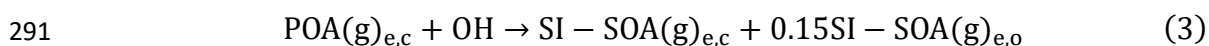
293 where POA(g) denotes primary organic aerosols with c* of 10^5 µg m^{-3}, which reacts

294 with OH to form SI-SOA(g) with c* of 10^{-2} µg m^{-3}. Subscripts c and o represent the

295 non-oxygen and oxygen parts respectively of given species and e is either the biomass

296 or anthropogenic emission sector. In addition, SVOC and IVOC emissions

297 corresponding to both anthropogenic and biomass burning emissions are derived based

298 on constant emission ratio of S/IVOC to POA ~~(Shrivastava et al., 2011). A detailed~~

299 ~~description of 2-species VBS mechanism can be found in Shrivastava et al.~~

300 ~~(2011)~~(Shrivastava et al., 2011). A detailed description of 2-species VBS mechanism

301 can be found in Shrivastava et al. (2011).

302 **2.3 Model sensitivity formulations**

303   Three sets of sensitivity tests are designed and listed in Table3. The purposes of

304 the three sets of experiments are as follows: (1) Adjust the condensation growth process

305 of ultrafine particles in WRF-Chem model (Base, MAC, ~~POA~~PEP, NOCD, RACD,

306 with details in Table 3).; (2) Explore the effect of SI-SOA yield on CCN (Low-_Yield

307 and High_Yield); (3) Study the effect of nucleation process on CCN under the change

308 of SI-SOA yield (Low-_Yield and High_Yield and their corresponding cases without

309 nucleation parameterization, i.e., Low_nucoff and High_nucoff). Each scenario will be

310 explained in conjunctions with the results.

334

Table 3 The sensitivity tests involved in this study

Purposes	Simulation scenarios	Description
Adjust the condensation growth process of ultrafine particles	Base	~~Simulation with the default setting with nucleation coefficient set as 2×10^{-6} s^{-1}, the same as Lai et al. (2022)~~ Simulation with the default setting with nucleation coefficient set as 2×10^{-6} s^{-1}, the same as Lai et al. (2022)
	Mass accommodation coefficient (MAC)	It is the same as Base except that the mass adjustment coefficient (α) of gaseous sulfuric acid is adjusted from 0.1 to 0.65.
	POA emission phase (PEP)	It is the same as MAC except that the phase of POA is changed from gas phase to particle phase.
	No condensation (NOCD)	It is the same as PEP except that no NH_4NO_3 condenses on particles below 40 nm.
	Ratio method for condensation	~~It is the same as PEP except that the condensation of NH_4NO_3 on~~

	(RACD)	~~particles below 40 nm is reduced according to the ratio of acid particles to total particles reported in Wang et al. (2014).~~It is the same as PEP except that the condensation of NH_4NO_3 on particles below 40 nm is reduced according to the ratio of acid particles to total particles reported in Wang et al. (2014).
Explore the effect of SI-SOA yield on CCN (Explore the effect of nucleation process on CCN under the change of SI-SOA yield)	High_Yield	Simulation with high oxidation rate of SI-SOA formation with reaction rate constant of 5×10^{-11} cm^3 $molec^{-1}$ s^{-1}
	Low-_Yield	Simulation with low oxidation rate of SI-SOA formation with reaction rate constant of 2×10^{-11} cm^3 $molec^{-1}$ s^{-1}
Explore the effect of nucleation process on CCN under the change of SI-SOA yield	High_NUCOFF	Simulations without nucleation parameterizations based on High_Yield
	Low_ NUCOFF	Simulations without nucleation parameterizations based on Low-_Yield

335

3. Results

3.1 Observational analysis

Based on the criteria ~~(Dal Maso et al., 2005; Kulmala et al., 2012)~~(Dal Maso et al., 2005; Kulmala et al., 2012), NPF is defined as an event with the emergence of a nucleation mode with particle diameters smaller than 25 nm, lasting for 2 hours or more, followed in general by a continuous particle growth. Six NPF events were identified in February 2017 in Qingdao, on the days of 6, 9, 10, 17, 20 and 23 (Fig. 1a), yielding a

frequency of ~30% and displaying a typical banana-shaped growth of particles in the particle number size distribution. Compared to a few other studies on NPF frequency in Qingdao, the results in this study are to a large extent consistent with that in the fall of 2012–2013 (30%; (Zhu et al., 2019)(Zhu et al., 2019)), slightly higher than that in summer 2016 (22%; (Zhu et al., 2019)(Zhu et al., 2019)) and lower than that in spring of 2010 (41%; (Liu et al., 2014c).(Liu et al., 2014c). The higher frequency in spring in Qingdao is consistent with the observational results at different stations in the Northern Hemisphere in Nieminen et al. (2018)Nieminen et al. (2018).
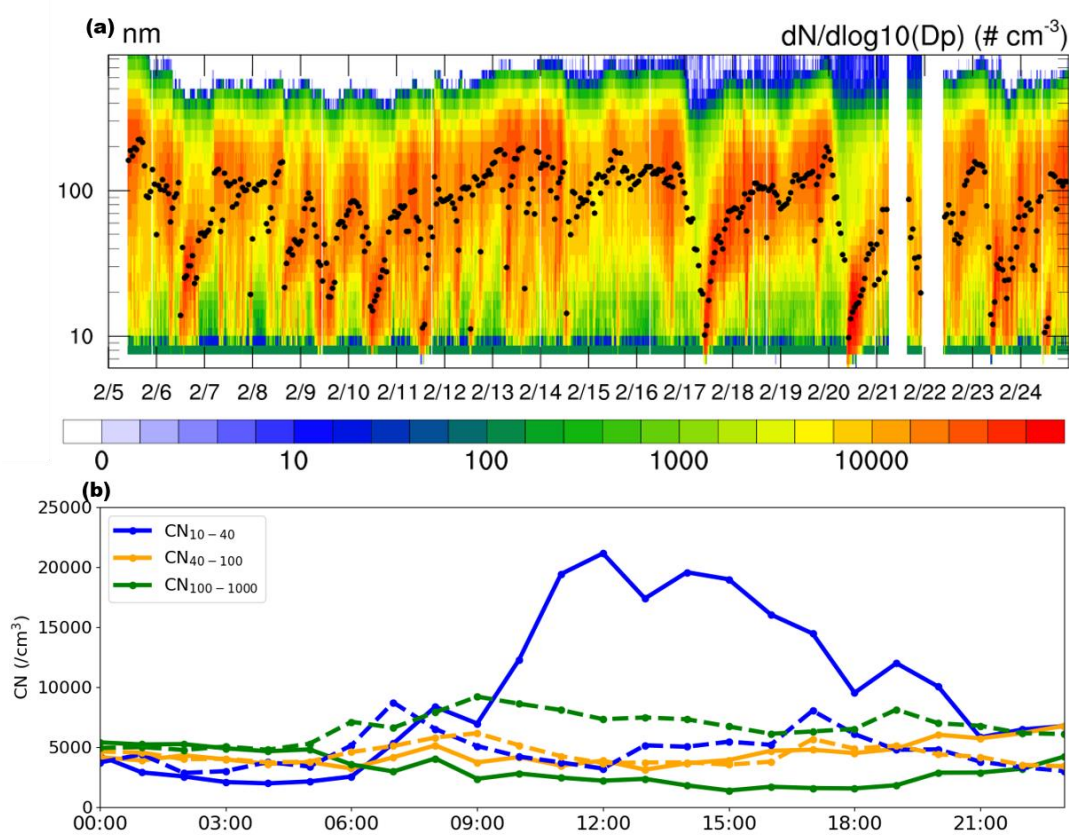
Fig. 1. Distribution of particle number concentration. (a) Temporal evolution of particle size distributions (colored shading) and geometric median diameter (GMD; dots in black) in Qingdao on February 5-24, 2017. (b) The mean diurnal variation of CN_{10-40} (blue), CN_{40-100} (orange) and $CN_{100-1000}$ (green) composited during the NPF (solid lines) and non-NPF (dashed lines) days on February 5-24, 2017. All times are local times (LT)

During the six NPF events identified in February in Qingdao, the mean diurnal cycle of CN_{10-40} (10–40 nm) particles exhibits triple peaks (solid blue in Fig. 1b), in the

morning (8:00 LT), noon (12:00–14:00 LT) and evening (19:00 LT), respectively. A comparable three-peak feature was also observed in earlier years during 2016-2018 in Qingdao ~~(Zhu et al., 2021)~~(Zhu et al., 2021). The morning and evening peaks of CN_{10-40}, with values of ~5300 cm^{-3} and ~12000 cm^{-3}, respectively, are likely caused by the primary emissions from traffic and cooking activities ~~(Wu et al., 2021a; Wang et al., 2022; Cai et al., 2020)~~(Wu et al., 2021a; Wang et al., 2022; Cai et al., 2020). The occurrence of NPF starts approximately at 9:00 am LT, accompanied by a substantial increase in CN_{10-40} compared with non-NPF days (solid vs. dashed lines, in blue), yielding a peak around noon (20000 cm^{-3} during 12:00–14:00 LT). In addition, larger particles (e.g., CN_{40-100} and $CN_{100-1000}$) displayed a slow or no increase in the afternoon.

3.2 Model improvement in particle number concentration simulations

Particle number concentrations, primarily in two ranges of 10–40 nm and 40–100 nm, are commonly simulated with large biases. In the smaller size range (10–40 nm), the particle number concentration is associated with NPF and particle growth. During NPF, despite differences among the formation mechanisms, H_2SO_4 is considered the common species ~~(Yu, 2005; Lovejoy et al., 2004)~~(Yu, 2005; Lovejoy et al., 2004), which often suffer large biases ~~(Cai et al., 2016; Matsui et al., 2011)~~(Cai et al., 2016; Matsui et al., 2011). In the size range of 40–100 nm, the particle number concentration is primarily affected by the condensation growth of particles below 40 nm, which is closely related to chemical components such as SOA and nitrate. Prior to the evaluation of particle number concentration, we first evaluate the compositions of $PM_{2.5}$ and criteria air pollutants including $PM_{2.5}$, PM_{10}, O_3, SO_2, CO, and NO_2, showing relatively low biases compared to observations (section S1 and Fig. S1 and Fig. S2 of the supporting information).

3.2.1 Bias correction of particle number concentration at 10–40 nm

In this study, as shown in Fig. 2, comparisons of CN_{10-40} between simulations (red line in Fig. 2a) and observations (black line in Fig. 2a) results of the six NPF events mentioned in the previous section in Qingdao in February 2017 indicate that model

390   overestimates CN_{10-40} with mean fractional bias of 48%. As one of the major processes

391   affecting the particle number concentration of 10–40 nm, nucleation is governed by the

392   particle nucleation rate of 1 nm particles $(cm^{-3} \, s^{-1})$, which is closely associated with the

393   concentration of H_2SO_4. For instance, in a commonly applied activation mechanism,

394   the nucleation rate calculated by $J^* = K_{ACT} \times [H_2SO_4]$. Note that K_{ACT} is the nucleation

395   coefficient considering the physical properties and chemical species of nucleation

396   process under different environments, indicating that a lumped chemical species are

397   included in the scheme reflected primarily in the nucleation coefficient k, set as 2×10

398    $^{-6} \, s^{-1}$ based on previous studies ~~(Sihto et al., 2006; Riipinen et al., 2007)~~(Sihto et al.,

399   2006; Riipinen et al., 2007)~~. Dong et al. (2019)~~. Dong et al. (2019) simulated NPF

400   occurring in the summer of 2008 in the United States using the NPF-explicit WRF-

401   Chem based on the activation mechanism, which overestimated the particle number

402   concentration at 10–63 nm by nearly doubled, even when the K_{ACT} decreased by one

403   order of magnitude (set at a very low value of $10^{-7} \, s^{-1}$). Therefore, it is likely that the

404   overestimation of particle number concentration in the smaller particle size segment is

405   probably due to the bias of simulated sulfuric acid.
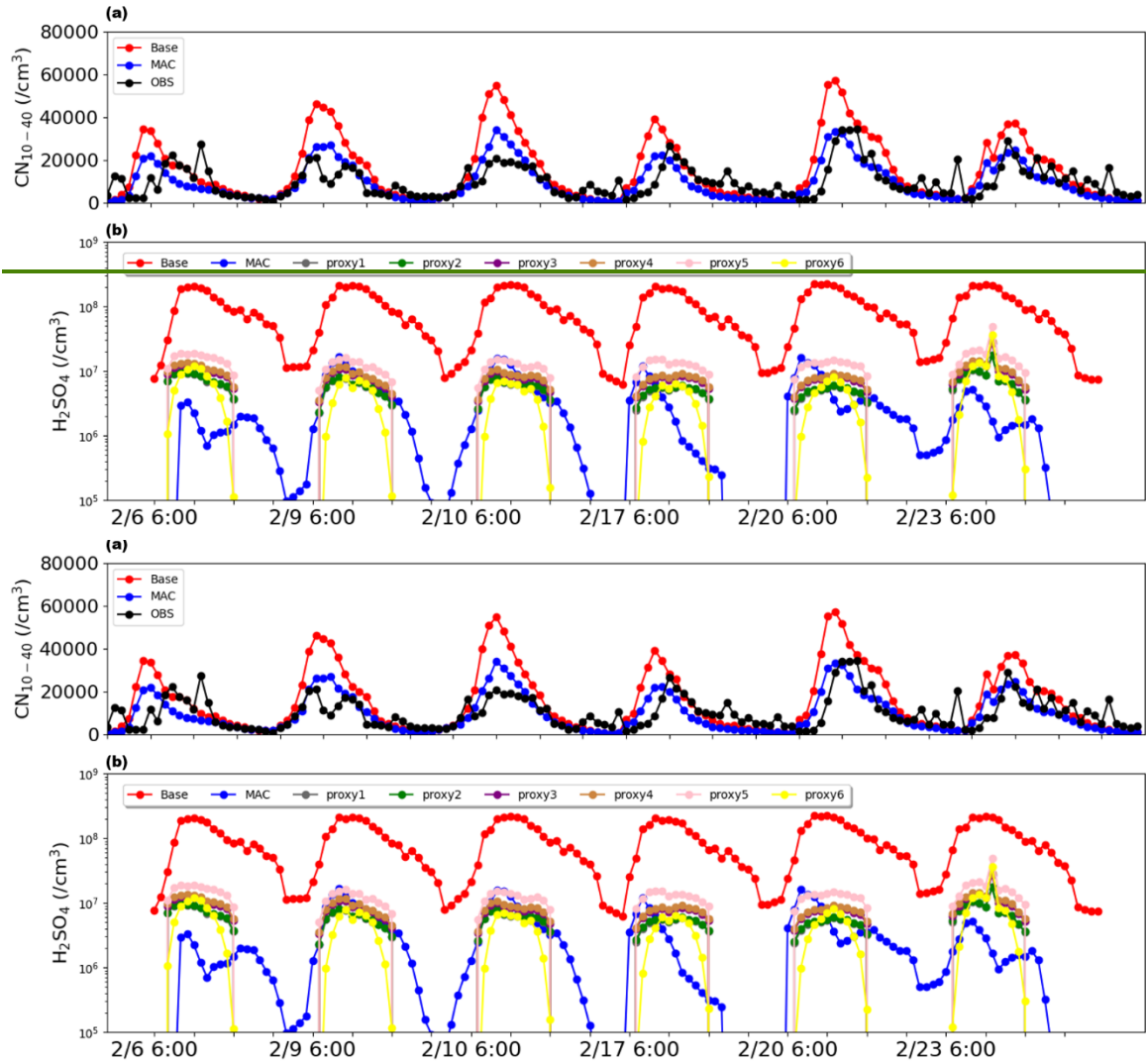
Fig. 2. Time series of (a) CN_{10-40} on NPF days, where red and blue represent Base and MAC simulation results respectively, and black represents observation results, and (b) sulfuric acid gas concentration obtained by simulation and by proxies (dark grey: Eq. 5; green: Eq. 6; purple: Eq. 7; brown: Eq. 8; pink: Eq. 9; yellow: Eq. 10). All times are in local times.

Measurement of sulfuric acid gases in the lower troposphere is challenging due to the generally low ambient concentration of sulfuric acid (10^6–10^7 molecule cm^{-3}). Different methods have been proposed to estimate ambient sulfuric acid concentrations based on observations such as SO_2 ~~(Petäjä et al., 2009; Lu et al., 2019; Mikkonen et al., 2011)~~(Petäjä et al., 2009; Lu et al., 2019; Mikkonen et al., 2011)~~. For instance, Petäjä et al. (2009)~~. For instance, Petäjä et al. (2009) proposed a linear method to approximate

420 observed H_2SO_4 concentration in ~~Hyytiala, southern Finland. Moreover, a recent study~~

421 ~~by Lu et al. (2019)~~Hyytiälä, southern Finland. Moreover, a recent study by Lu et al.

422 (2019) proposed a nonlinear method to construct a number of proxies for gaseous

423 sulfuric acid concentration (Eq. 5–9), indicating that compared to the linear method in

424 ~~Petäjä et al. (2009)~~Petäjä et al. (2009), the nonlinear relationship can provide more

425 accurate H_2SO_4 concentration in Beijing during February–March 2018 period. In

426 addition, we also used another sulfuric acid nonlinear proxy (Eq. 10) based on long-

427 term observations in Germany, Finland, the United States, etc. ~~(Mikkonen et al.,~~

428 ~~2011)~~(Mikkonen et al., 2011). In this study, we adopt the above six nonlinear proxy

429 methods (referred as proxy5 to proxy10) to estimate H_2SO_4 in Qingdao.

430 $$[H_2SO_4] = 515.74 \times [SO_2]^{0.38} \times \text{Radiation}^{0.14} \times CS^{0.03} \qquad (5)$$

431 $$[H_2SO_4] = 280.05 \cdot \text{Radiation}^{0.14}[SO_2]^{0.40} \qquad (6)$$

432 $$[H_2SO_4] = 9.95 \times [SO_2]^{0.39} \times \text{Radiation}^{0.13} \times CS^{-0.01} \times [O_3]^{0.14} \qquad (7)$$

433 $$[H_2SO_4] = 14.38 \times [SO_2]^{0.38} \times \text{Radiation}^{0.13} \times [O_3]^{0.14} \qquad (8)$$

434 $$[H_2SO_4] = 0.0013 \times [SO_2]^{0.38} \times \text{Radiation}^{0.13} \times CS^{-0.17} \times ([O_3]^{0.14} + [NO_x]^{0.41}) \quad (9)$$

435 $$[H_2SO_4] = 8.21 \times 10^{-3} \times [SO_2]^{0.62} \times \text{Radiation} \times (CS \times RH)^{-0.13} \qquad (10)$$

436 where $[SO_2]$, $[O_3]$ and $[NO_x]$ (molecule cm^{-3}) represents concentration of

437 observed SO_2, O_3 and NO_x, respectively. "Radiation" (W m^{-2}) is global radiation. RH

438 (%) is the relative humidity, and CS (s^{-1}) is the condensation sink, which is calculated

439 based on observed particle distribution.

440

441 The simulated H_2SO_4 concentration from the Base simulation (dots in Fig. 2b) is

442 compared with observations obtained by proxies (see Fig. 2b), indicating that Base

443 simulations apparently overestimate by one order of magnitude compared to the H_2SO_4

444 estimated by proxies. The overestimation has been frequently reported previously, i.e.,

445 over Beijing ~~(Matsui et al., 2011)~~(Matsui et al., 2011), which ascribes the bias to the

446 overestimation of the SO_2 concentration. In a more recent study, the sensitivity of

447 H_2SO_4 to SO_2 is tested, and the result shows that even when SO_2 is reduced to an

448 unrealistically low level, the simulated H_2SO_4 is still more than one order of magnitude

higher than the observed value (Lai et al., 2022), suggesting that the SO_2 concentration cannot fully explain the overestimates.

In addition to the precursor of H_2SO_4, the mass accommodation coefficient (α), representing the probability of impaction of a gaseous molecule on a liquid surface and entering the bulk liquid phase, is another important factor affecting the concentration of sulfuric acid gas. In the public release of WRF-Chem, mass accommodation coefficient is typically set to a low value of 0.1 for all gas species under different volatility during the condensation process, including H_2SO_4 ~~(Davidovits et al., 2004; Zaveri et al., 2008)~~(Davidovits et al., 2004; Zaveri et al., 2008). Recent studies indicate that the low mass accommodation coefficient value may not be applicable to the low volatile gases, which tend to have a mean mass accommodation coefficient value of 0.7 and close to the unity ~~(Krechmer et al., 2017)~~(Krechmer et al., 2017). In fact, an earlier study has indicated based on experimental determination, the mass accommodation coefficient of H_2SO_4 vapor in sulfuric acid aqueous solution was measured, and the best fit value was 0.65 ~~(Pöschl et al., 1998)~~(Pöschl et al., 1998). Accordingly, a sensitivity simulation was conducted by adjusting the mass accommodation coefficient of H_2SO_4 from 0.1 to 0.65, referred to as MAC.

This simulation brought the H_2SO_4 concentration (see Fig. 2b) much closer to the calculated results from proxies, and the corresponding biases reduced by approximately an order of magnitude. Notably, the MAC simulation decreases the overestimate of sulfuric acid gas concentration, resulting in a lower particle formation rate. The MAC simulation also significantly reduces overestimate of CN_{10-40} (Fig. 2a), and mean fractional bias compared to observations decreases from 48% to 1%.

3.2.2 Improvement of particle number concentration simulations at 40–100 nm

The number concentration of particles in the 40–100 nm range is mainly affected by the coagulation and condensation processes. While the coagulation process tends to largely affect ultrafine particles below 10 nm than those with larger sizes ~~(Wu et al., 2011)~~(Wu et al., 2011), the condensation growth of particles during gas-particle partitioning at sizes of 10–40 nm, to a large extent, governs the variations in number

concentration of 40–100 nm particles. The condensation process is primarily controlled by gas-particle partitioning of chemical species, which may change the chemical composition of particles, such as organic compounds and inorganics including sulfate, nitrate and ammonium.

Among the species contributing to the condensation growth of particles at 10–40 nm, the organic compounds with $c*$ of 10^{-2} µg m^{-3} play the dominant role ~~(Pierce et al., 2011)~~(Pierce et al., 2011). In the current model setting, the low volatile organic matter of 10^{-2} µg m^{-3} comes from two gas-phase sources, including the direct emission of primary organic aerosol (POA) and SOA formed from S/IVOC (SI-SOA), conducive to condensation on particles. While the condensation of gaseous SOA is in general reasonable, the gas phase emissions of POA may be problematic. For instance, previous studies suggested that POA is in gas phase close to the emissions source. However, with rapid dilution and cooling in the atmosphere away from the source, most POA condenses to particle-phase ~~(Roldin et al., 2011b; Roldin et al., 2011a; Shrivastava et al., 2008)~~(Roldin et al., 2011b; Roldin et al., 2011a; Shrivastava et al., 2008). Therefore, away from the emissions source POA, being in the particle phase, will not be involved in the growth of newly formed particles. Therefore, POA may not contribute to particle growth away from the emission sources, which caused different size distributions of POA compared to when it was emitted in the gas-phase (Fig. S3a vs. Fig. S3b). Emitting low volatility POA in the particle phase eliminates the unreasonable quasi-banana shape pattern exhibiting concomitant growth of newly formed particles with increasing mass concentration of POA.

The composition analysis (Fig. S3c) in the 10–40 nm particles mass from the model results indicates that organic compounds mentioned above only account for 21% of total mass (sulfates, nitrates, ammonium salts and organics) in this size range and the dominant species is nitrate which accounts for 51% of total mass, exhibiting inconsistencies with the previous studies which in general indicates a much smaller contribution of nitrate. For instance, ~~Liu et al. (2014a)~~Liu et al. (2014a) suggested that over North China Plain in summer 2009, organic matter accounted for 77% of particles around 30 nm, while the sum of SO_4^{2-}, NO_3^- and NH_4^+ only accounted for 18%. Recent

observations conducted in Beijing also indicated that particles at 8–40 nm are mainly composed of organic matter (with mass fraction of ~80%) and sulfate (with mass fraction of ~13%), while nitrate content is very low (with mass fraction of ~3%) (Li et al., 2022). Another study showed that nitrate accounted for 7–8% at urban sites and 17% at rural sites for particles mass in 7–30 nm in the United States in 2007 ~~(Bzdek et al., 2012)~~(Bzdek et al., 2012). Therefore, the potentially too high modeled nitrate fraction in 10–40 nm in this study is tightly associated with the condensation process, with the specific reasons explained below.

The condensation of nitric acid on particles is highly constrained by the particle acidity. The acidity in smaller particles (i.e., 10–40 nm) tends to be higher than that in large particles, primarily due to the larger condensation of H_2SO_4 ~~(Lu et al., 2022)~~(Lu et al., 2022), and particles with sizes greater than 40 nm have a much weaker acidity or are nearly neutral. For example, observed evidence has shown that acidic ultrafine particles account for a large proportion of ultrafine particles from 22 December 2010 to 15 January 2011 in Hong Kong, e.g., 65% for particles within 5.5–30 nm ~~(Wang et al., 2014)~~(Wang et al., 2014).

In the model, a particle is determined to be in solid phase when the ambient relative humidity is lower than the mutual deliquescence relative humidity of the particles ~~(Zaveri et al., 2005; Zaveri et al., 2008)~~(Zaveri et al., 2005; Zaveri et al., 2008), which is in general suitable for particles dominated by inorganics. In the study area, the results indicate that at most conditions relative humidity are relatively low and the particles are in solid phase, in which the condensation process is not affected by particle acidity and the condensation of nitric acid on particles is directly calculated based on the gas-particle equilibrium concentration ~~(Zaveri et al., 2008)~~(Zaveri et al., 2008). However, for particles below 40 nm, the main compositions are likely to be organic matter ~~(Zhu et al., 2014; Ehn et al., 2014)~~(Zhu et al., 2014; Ehn et al., 2014), which tends to be in liquid phase ~~(Virtanen et al., 2011; Cheng et al., 2015)~~(Virtanen et al., 2011; Cheng et al., 2015), under which the condensation of nitric acid is strongly constrained by acidity. Therefore, the phase misrepresentation ignores the weakening effect of acidity on nitric acid condensation, resulting in too high nitrate therein.

To overcome this issue, we propose a ratio method for condensation (RACD) to partition the condensation of nitric acid on particles under 40 nm, by applying a ratio of the number concentration of non-acidic particles to ultrafine particles. The method is based on two assumptions, including: 1) little condensation of nitric acid on particles with strong acidity (Lu et al., 2022)(Lu et al., 2022); 2) the condensation of nitric acid on particles is proportional to the ratio of the number concentration of non-acidic ultrafine particles to the total particles, despite the existence of uncertainties. Fig. S4 depicts the average particle number concentration and acid particle in the 1 to 40 nm range, calculated based on Wang et al. (2014)Wang et al. (2014). The ratio of non-acidic particles is 8% for particles below 10 nm, 18% for particles at 10–15.8 nm, 30% for particles at 15.8–25.1nm, and 55% for particles at 25.1–39.8 nm (Fig. S4). Note that the ratio is based on measurements acquired at a single site in Hong Kong, therefore more observational studies are needed to warrant the robustness of the method. Alternatively, the condensation of nitric acid on particles in bins from 1nm to 40 nm is completely suppressed, referred to as NOCD.

The simulation results based on the two methods (RACD and NOCD) are shown in Fig. 3. Compared to MAC, RACD simulations reduce previously noted overestimation of particle number concentration in the 40–100 nm size range (Fig. 3b), with the mean fractional bias decreases from 83% to 63%. In addition to the amount of nitrate condensation during particle growth mentioned above, the overestimation of particle number concentrations in the 40–100 nm range may be attributed to nucleation process. More specifically, in the H_2SO_4-H_2O binary nucleation mechanism used in this study, when the concentration of sulfuric acid gas is reduced (Section 3.2.1), the resulting decrease in nucleation rate leads to a slight decrease in particle number concentration at 40–100 nm relative to Base (mean fractional bias from 98% to 83%). Apart from that, it may also be related to the choice of nucleation parameterization scheme. For example, using a global chemical transport model GEOS-Chem with a nucleation mechanism in which formation rate is a function of the concentrations of sulfuric acid and low-volatility organics, Yu et al. (2015)Yu et al. (2015) overestimated the concentration of particles in the 10–100 nm range by 161% at nine sites in the summer in North America.

569 A possible explanation for this overestimation was given by the uncertainty of the

570 predicted concentration of organic compounds involved in organics-mediated

571 nucleation parameterization. After they switched to another scheme of the ion-mediated

572 nucleation mechanism without organic matter, the number becomes 27% lower than the

573 observations ~~(Yu et al., 2015)~~(Yu et al., 2015). The test based on different schemes is

574 beyond the scope of the study, which is therefore not investigated.

575 Moreover, the overestimation of particles over 100 nm ($CN_{100-1000}$; Fig. 3c), which

576 have a strong influence on CCN, also decrease in the RACD simulation. Thus, the mean

577 fractional bias decreases from 25% (MAC) to 1%. Note that the slight increase of CN_{10-40}

578 through the application of RACD, can be linked to the decrease of nitrate

579 condensation, and leads to weakened particle growth and enhanced particle number

580 concentration at 10–40 nm (Fig. 3a). The alternative method by completely removing

581 the nitrate condensation (NOCD) yields even better performance in particle number

582 concentration of 40–100 nm (mean fractional bias of 34%), indicating the feasibility by

583 reducing the nitrate condensation. The proportion of nitrate simulated by RACD is 23%,

584 closer to values reported in past observations ~~(Bzdek et al., 2011; Bzdek et al.,~~

585 ~~2012)~~(Bzdek et al., 2011; Bzdek et al., 2012), while the nitrate (1%) in the scenario of

586 NOCD seems to be too low. Considering the limited observational information obtained

587 based on previous studies, RACD is applied in this study.

588 In addition to Qingdao, we evaluate the model performance over a few other sites,

589 including one site over urban Beijing and the other one over the rural area of Gucheng,

590 yielding consistent improvements in model simulations (Section S2; Fig. S6-S8).

591 Moreover, we select another empirical scheme, e.g., kinetics, and one classical

592 nucleation scheme, indicating the empirical scheme of activation scheme is in general

593 a good option in this study (Section S2; Fig. S9-S11; Table S1-3).
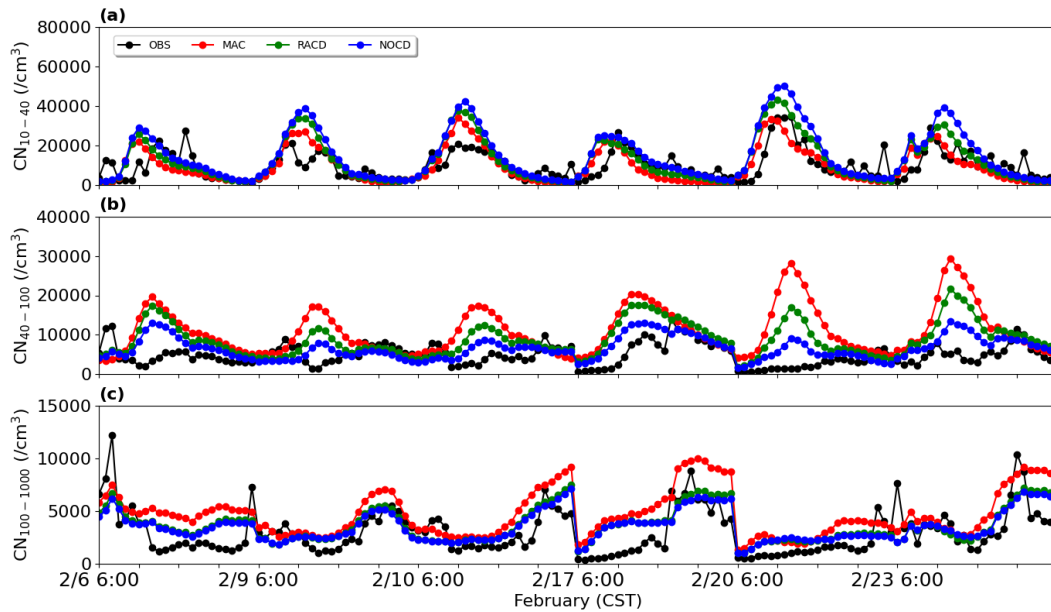
Fig. 3. The time series of (a) CN_{10-40}, (b) CN_{40-100} and (c) $CN_{100-1000}$ on NPF days in Qingdao on February 5-24 simulated from MAC (marked in red), NOCD (marked in blue) and RACD (marked in green) as well as from observations (OBS) (marked in black). All times are local time.

3.3 Substantial contributions of SI-SOA to CCN

Compared with the original model setting, after adjusting the growth process of ultrafine particles (RACD), the number concentration of particles ~~tend~~tends to decrease, especially for particles above 40 nm. Ultrafine particles above 40 nm are important sources of CCN ~~(Dusek et al., 2006)~~(Dusek et al., 2006), in this way, the number concentration of CCN also tends to decline. In addition, in the Base case, we found that the model overestimated $CCN_{0.4\%}$ and $CCN_{0.6\%}$, with mean fractional bias being 64% and 87%, respectively. After adjusting the condensation growth process of ultrafine particles, under high supersaturation (i.e., $CCN_{0.4\%}$ and $CCN_{0.6\%}$), the capability of the model in reproducing the CCN is improved. RACD reduces the overestimation of $CCN_{0.4\%}$ and $CCN_{0.6\%}$, with mean fractional bias reduced to 30% and 56%, respectively, although the overestimates still exist (Figs. S5b, c). However, for low supersaturation (i.e., $CCN_{0.2\%}$), the decrease of number concentration of CCN is too large, and mean

614 fractional bias decreases from 7% to -45% (Fig. S5a), therefore the bias will be further

615 adjusted later.

616   In addition to the growth process, the remaining overestimate of CCN under high

617 SS and underestimate of CCN over low SS is likely to be influenced by the chemical

618 compositions involved in the activation of ultrafine particles into CCN. Specifically,

619 ultrafine particles can grow up to CCN size under certain SS (Pierce and Adams, 2007).

620 This process is influenced by both particle size and hygroscopicity, and hygroscopicity

621 is closely related to the chemical composition of particles (Petters and Kreidenweis,

622 2007). In particular, inorganic compounds generally increase particle hygroscopicity,

623 increasing CCN. SOA has dual effects on CCN since it decreases particle

624 hygroscopicity but also promotes growth of particles, and these two effects are

625 competitive with each other (Wu et al., 2015; Zaveri et al., 2021). Ultrafine particles

626 must grow to a critical size to be activated into CCN (Dusek et al., 2006)(Dusek et al.,

627 2006). SOA act as a major contributor in promoting the condensational growth of

628 ultrafine particles to the critical size, facilitating particles activation into CCN. In

629 contrast, SOA tends to reduce the hygroscopicity of particles, leading to a diminished

630 ability of activation to CCN (Wu et al., 2015). These two competing effects work

631 together and modulate the number of CCN. Moreover, considering that SI-SOA is the

632 main SOA component on ultrafine particles (Fig. S5d), the effect of SI-SOA on CCN is

633 therefore explored in this study.

634   Considering SI-SOA is a product of S/IVOC oxidation, the oxidation rate of

635 S/IVOC is tightly associated with CCN, which likely affects the bias of CCN. In the

636 original model setup, the oxidation rate is set to be a constant of 4×10^{-11} cm^3 molec^{-1}

637 s^{-1} for all S/IVOC. However, a recent study (Wu et al., 2021b)However, a recent study

638 (Wu et al., 2021b) proposed that the oxidation rate can be as high as 5×10^{-11} cm^3 molec^{-1}

639 ^{1} s^{-1} such as for polycyclic aromatic hydrocarbons (PAHs), close to the original model

640 value, but can be as low as half (i.e., 2×10^{-11} cm^3 molec^{-1} s^{-1}) of the original modeling

641 setting for S/IVOC species except PAHs (O-S/IVOCs). It is noteworthy that the

642 oxidation rates of 5×10^{-11} and 2×10^{-11} in general represent the upper and lower bounds

643 (Zhao et al., 2016; Wu et al., 2021b)(Zhao et al., 2016; Wu et al., 2021b).

To delve into how oxidation rates affect CCN, we set up a few numerical experiments (Table 2̶3) to investigate the response of CCN to the oxidation rate of S/IVOC at three supersaturations (0.6%, 0.4%, 0.2%), including cases of High_Yield and Low_Yield. As it is shown in Fig. 4, decreasing the oxidation rate (Low_Yield) leads to a reduction of ~10% of CCN at high supersaturation (i.e., CCN0.6%) as compared to the High_Yield simulation. This behaviour is a consequence of the decrease of particle number concentrations associated with Low_Yield, particular of the particles close to the critical diameter (40–100 nm). In this case, the effect of particle size dominates the hygroscopicity. In contrast, at a lower supersaturation (CCN$_{0.2\%}$), CCN increases by 42% when the oxidation rate is switched from a high to a low value, which is due to the smaller fraction of SI-SOA contributing to particulate mass when the oxidation rate is low. In this case, relative to SOA, a larger fraction of other particle constituents such as inorganics, increase the volume weighted particle hygroscopicity (̶D̶u̶s̶e̶k̶ ̶e̶t̶ ̶a̶l̶.̶,̶ ̶2̶0̶0̶6̶)̶(Dusek et al., 2006) which causes the increase of CCN number. This means that the effect of hygroscopicity on CCN surpasses the influence on particle size at low supersaturations. This conclusion is consistent with the observation conducted by M̶a̶ ̶e̶t̶ ̶a̶l̶.̶ ̶(̶2̶0̶1̶6̶)̶Ma et al. (2016) in the North China Plain in 2013, which suggested that along with the decrease of SS, the particles that can be activated to CCN is more sensitive to changes of particle hygroscopicity. Similarly, based on observational data in northern China in summer, Wang et al. (2023) found that CN in 2020 is lower than that in 2014 due to particulate pollution control, however, the particles become more easily activated, attributable to the larger extent of decrease in organic matters compared to inorganics, leading to enhanced particle hygroscopicity and more conducive to activation.
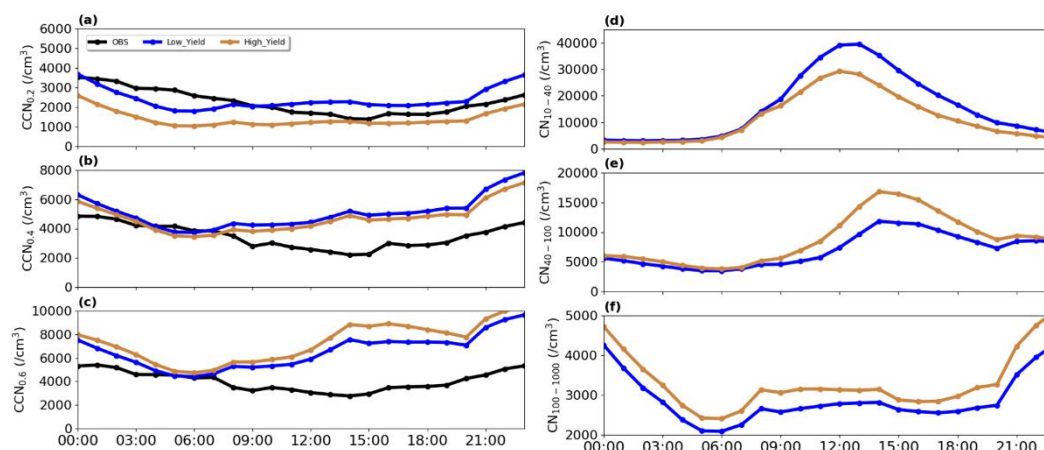
692

693 Fig. 4. Average diurnal variation of (a) $CCN_{0.2\%}$, (b) $CCN_{0.4\%}$ and (c) $CCN_{0.6\%}$ and (d)

694 $CN_{10–40}$, (e) $CN_{40–100}$, (f) $CN_{100–1000}$ on NPF days in Qingdao on February 5-24, 2017,

695 in Low_yield and High_yield simulations, shown as blue and brown lines, and black

696 lines represent observation results.

697

698 Furthermore, compared to the high yield of SI-SOA, the low SI-SOA yield results

699 in a high CCN concentration under low SS and low CCN concentration under high SS.

700 Therefore, both the underestimates of $CCN_{0.2\%}$ (mean fractional bias of -45%) and

701 overestimates of $CCN_{0.6\%}$ (mean fractional bias of 56%) mentioned above are improved,

702 with mean fractional bias of $CCN_{0.2\%}$ and $CCN_{0.6\%}$ reaching 7% and 43%, respectively

703 (Fig. 4a,c). This result suggests that the oxidation rate of S/IVOC is possibly closer to

704 the low value, which is understandable based on ~~Wu et al. (2021b)~~Wu et al. (2021b),

705 who found that the amount of O-S/IVOCs, which corresponds to a low oxidation rate,

706 is in general much larger (i.e., 20 times) than that of PAHs with a high oxidation rate.

707 In addition to the single site of Qingdao, we further explore the impact of SI-SOA

708 yield on CCN from a larger spatial coverage (Fig. 5). Consistent with the mechanism

709 revealed over Qingdao, even from a larger spatial perspective, a lower oxidation rate of

710 S/IVOC essentially enhances CCN at a lower SS (e.g., $CCN_{0.2\%}$; Fig. 5a) with the

711 highest increase over North China Plain area (Fig. 5a), and weakens CCN (i.e., by 10–

712 20% over Beijing-Tianjin-Hebei) at a higher SS (Fig. 5c), particularly over the dense

713 emission area (Fig. S12). It is worth noting that in the 2-species VBS mechanism used

714 in our study, all S/IVOC in the inventory is calculated based on a constant emission

ratio of S/IVOC to POA from all source categories ~~(Shrivastava et al., 2011)~~(Shrivastava et al., 2011), which may miss part of S/IVOC due to different emission ratios of POA from different source ~~(Chang et al., 2022)~~(Chang et al., 2022). In addition, the simplified VBS mechanism used in our study does not take into account the multi-step oxidation of organic species, which may introduce some uncertainties. To be more specific, in the 2-species VBS mechanism, SI-SOA with effective saturation concentrations ($c*$) of 10^{-2} µg m^{-3} is formed by the vapor phase oxidation of S/IVOC vapors with $c*$ of 10^5 µg m^{-3}, reducing volatility by 7 orders of magnitude. The process of one-step oxidation does not mean to represent a physical process, but to parameterize the mean effect of a complex process of SOA formation (Shrivastava et al., 2011). However, in the real atmosphere, the gaseous VOCs often undergo multi-generational oxidation to form SOA (Garmash et al., 2020), during which the properties and composition of SOA change substantially. For instance, by adding the formation chemistry associated with multi-generational oxidation, Zhao et al. (2020) found improved simulations of vertical aerosol profile in the Amazon free troposphere compared to the simplified VBS mechanism.
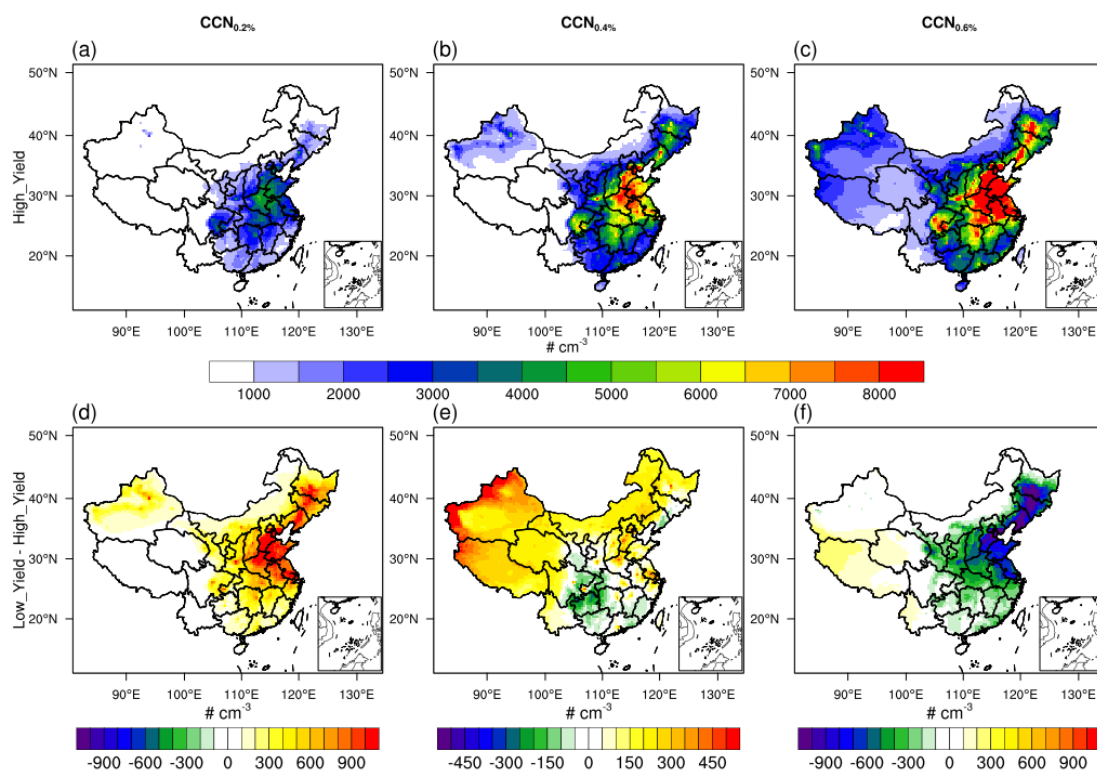
Fig. 5. Spatial distributions of CCN concentrations at different supersaturations (SS),

(a) and (d) are $CCN_{0.2\%}$, (b) and (e) are $CCN_{0.4\%}$, and (c) and (f) are $CCN_{0.6\%}$. The top panels exhibit the results from the High_Yield simulation, and the bottom panels shows the difference between the Low_Yield and High_Yield simulations.

3.4 Contribution of nucleation to CCN under different SI-SOA yields

Considering the importance of nucleated particles on CCN ~~(Yu et al., 2020; Westervelt et al., 2013)~~(Yu et al., 2020; Westervelt et al., 2013), we further investigate the influence of nucleation on CCN under different SI-SOA yield conditions discussed above.

As shown in Fig. 6, in simulations close to the original model setting (High_Yield), when SS is low (i.e., SS=0.2%), the nucleation process tends to reduce the CCN by ~10–50%. In contrast, when the SS is high (0.6%), the nucleation results in a significant increase in CCN in most regions of China. When the yield of SI-SOA is adjusted to a lower level, the nucleation process has a positive contribution to CCN under both low and high SS. Especially, when SS is low (0.2%), the sign reversal, i.e., from negative (Fig. 6a) to positive (Fig. 6d) contributions of NPF to CCN along with the decrease of SI-SOA yield, i.e., the increase is concentrated in the eastern China with an average of 10–20%. The primary mechanism lies in that along with the decrease of SI-SOA yield, the smaller fraction of SI-SOA yields an increase in hygroscopicity, which surpasses the suppression effect on particle growth due to reduced SI-SOA formation. In the real atmosphere, when the supersaturation is usually low, e.g. about ~0.1% in polluted areas ~~(Kalkavouras et al., 2019; Hudson and Noble, 2014)~~(Kalkavouras et al., 2019; Hudson and Noble, 2014), CCN will likely reduce with increasing oxidation rate of S/IVOC and corresponding SI-SOA formation.
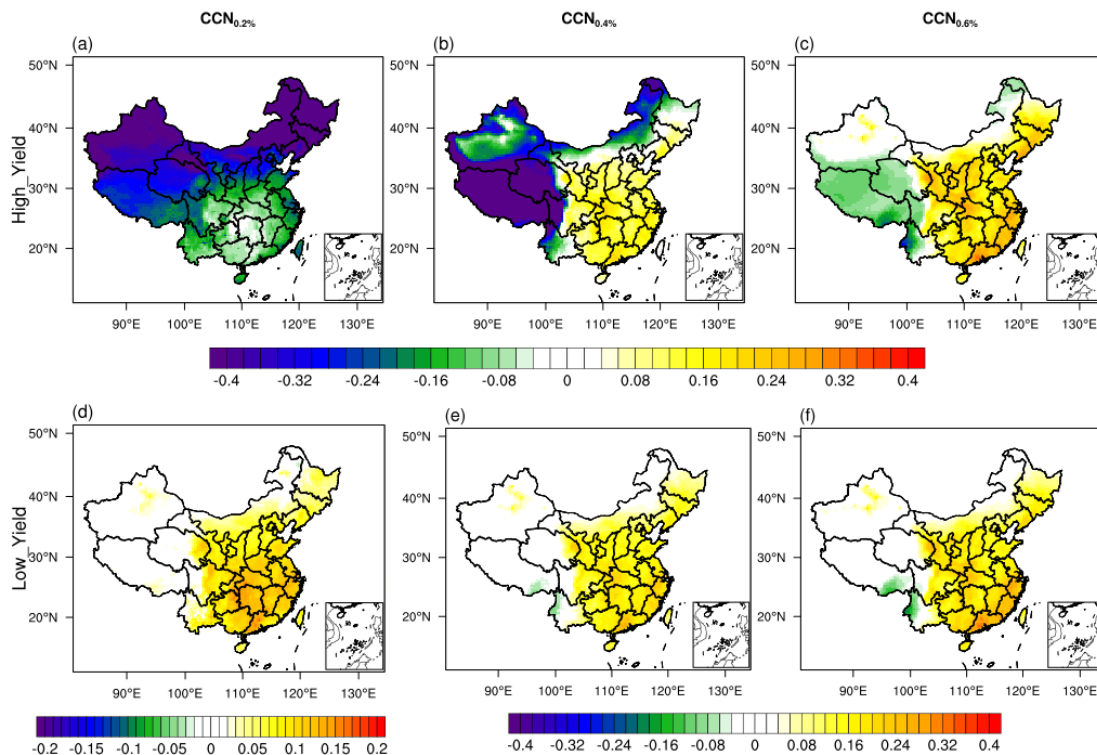
Fig. 6. Spatial distribution of contribution of nucleation to CCN calculated by the ratio of the difference between the parameterization with and without nucleation to the parameterization with nucleation under different SI-SOA yields in China in February 2017. (a), (d) is $CCN_{0.2\%}$, (b), (e) is $CCN_{0.4\%}$, (c), (f) is $CCN_{0.6\%}$. The upper panel and lower panel represent High_Yield and Low_Yield simulation respectively

In addition to the linear-H_2SO_4 nucleation mechanism, one more empirical scheme of kinetics nucleation is selected, which assumes that the nucleation rate is proportional to the square of the concentration of sulfuric acid ($J = K[H_2SO_4]^2$), to investigate the effect of nucleation on CCN. Substantially positive contributions of nucleation to CCN is found when the low SI-SOA yield is applied, consistent with what was shown based on the linear-H_2SO_4 nucleation scheme (Fig. S13). However, nucleation contributes positively to CCN even when the SI-SOA yield is high in the quadratic-H_2SO_4 nucleation scheme (e.g., kinetics nucleation scheme). When more sulfuric acid molecules participate in nucleation under this scheme than the linear-H_2SO_4 nucleation scheme, the particles are more easily hygroscopically activated to CCN, which is equivalent to the effect of a reduction in organic components in the linear-H_2SO_4

794   nucleation scheme (e.g., activation-type nucleation scheme). The results from this study

795   show the importance of assessing the simulated effects of the nucleation scheme on not

796   only the formation and growth process of particles but also climate factors such as CCN

797   using observations.

798

799 Conclusions and discussions

800   In this study, WRF-Chem explicit-NPF simulations, with linear-H_2SO_4 nucleation

801   scheme (e.g., activation-type nucleation scheme), are used to investigate the observed

802   wintertime NPF events and their contribution to CCN in China. Based on observations

803   in a typical coastal city of Qingdao, as well as in the cities of Beijing and Gucheng over

804   North China Plain, we identify high biases of the model simulated CN and CCN

805   concentrations. Therefore, we updated and improved the parameterization setting on

806   particle growth in the model, mainly including: (1) adjusting the mass accommodation

807   coefficient (α) to from the default value of 0.1 to 0.65, an important parameter for

808   sulfuric acid condensation; (2) proportionally reducing the condensation amount of

809   nitric acid on particles below 40 nm, (3) changing the emitted low-volatility POA from

810   gas to particle. Through these adjustments, the capability of the model in reproducing

811   CN and CCN is substantially improved, leading to better agreement with the observed

812   results, which significantly reduces the overestimation of CN_{10-40} (mean fractional bias

813   decreases from 48% to 1%) and CN_{40-100} (mean fractional bias decreases from 98% to

814   63%).

815

816   For CCN, due to the crucial role of SI-SOA in promoting the growth of ultrafine

817   particles, on the basis of previous studies, we lower the oxidation rate of S/IVOC and

818   hence the production rate of SI-SOA, which weakens the growth of particles to reach

819   the critical size of CCN activation, but enhances particulate hygroscopicity favoring the

820   activation to CCN. When the yield of SI-SOA is adjusted to the lower bound of

821   literature value, $CCN_{0.6\%}$ is reduced by ~10% and is closer to observations. At low SS

822   ($CCN_{0.2\%}$), the decrease of SI-SOA yield has greater effects on the increase of particle

823   hygroscopicity compared to the effect of the reduction of particle size due to the

decrease of condensation growth. It results in an increase of CCN (as large as ~42%) in better agreement with observations. Under low SS conditions, common in the atmosphere, a 2.5-fold reduction in SI-SOA yield results in a substantial increase of CCN that switches from a negative contribution of new particle formation to CCN from -50%~-10% to a positive contribution of 10~20%. ~~The substantial contribution of new particle formation to CCN under low SS and SI-SOA is applicable to other mechanisms such as kinetics.~~

In addition to activation nucleation scheme, we have also tested a few other schemes such as the quadratic-H_2SO_4 nucleation scheme (e.g., kinetics nucleation scheme). Under this scheme, the bias-corrected method abovementioned is applicable to improving the simulations of concentrations of CN and CCN. It is noteworthy that the dependence of CCN on the SI-SOA yield is diminished, showing that under both high and low yields of SI-SOA, there are positive contributions of NPF to CCN. This is likely due to the increase in the amount of sulfuric acid involved in nucleation, making it more hygroscopic and easier to activate to CCN, and the high content of inorganic species makes them less sensitive to changes in SI-SOA yield, which deserves further investigation.

Competing interests. At least one of the (co-)authors is a member of the editorial board of Atmospheric Chemistry and Physics.

Acknowledgements. This research was supported by grants from the National Natural Science Foundation of China (42122039) and Fundamental Research Funds for the Central Universities (202072001). Y.W. was supported by the National Science Foundation Atmospheric Chemistry Program. M.S. was supported by the U.S. Department of Energy (DOE) Office of Science, Office of Biological and Environmental Research (BER) through the Early Career Research Program and the Atmospheric System Research (ASR) program.

References:

854 Arghavani S, Rose C, Banson S, et al. 2022. The Effect of Using a New Parameterization of Nucleation
855   in the WRF-Chem Model on New Particle Formation in a Passive Volcanic Plume. Atmosphere
856   [J], 13(1): 15.
857 Bergman T, Laaksonen A, Korhonen H, et al. 2015. Geographical and diurnal features of amine-enhanced
858   boundary layer nucleation. Journal of Geophysical Research: Atmospheres [J], 120(18): 9606-
859   9624.
860 Buchholz R R, Emmons L K, Tilmes.S 2019. The CESM2 Development Team., 2019. CESM2.1/CAM-
861   Chem Instantaneous Output for Boundary Conditions. UCAR/NCAR - Atmospheric Chemistry
862   Observations and Modeling Laboratory.
863 Bzdek B, Zordan C, Luther G, et al. 2011. Nanoparticle Chemical Composition During New Particle
864   Formation. Aerosol Science and Technology [J], 45(1041-1048.
865 Bzdek B R, Zordan C A, Pennington M R, et al. 2012. Quantitative Assessment of the Sulfuric Acid
866   Contribution to New Particle Growth. Environmental Science & Technology [J], 46(8): 4365-
867   4373.
868 Cai C, Zhang X, Wang K, et al. 2016. Incorporation of new particle formation and early growth
869   treatments into WRF/Chem: Model improvement, evaluation, and impacts of anthropogenic
870   aerosols over East Asia. Atmospheric Environment [J], 124(262-284.
871 Cai J, Chu B, Yao L, et al. 2020. Size-segregated particle number and mass concentrations from different
872   emission sources in urban Beijing. Atmos. Chem. Phys. [J], 20(21): 12721-12740.
873 Carter W 2000. Documentation of the SAPRC-99 Chemical Mechanism for VOC Reactivity Assessment.
874   Final Report to California Air Resources Board [J].
875 Chang X, Zhao B, Zheng H, et al. 2022. Full-volatility emission framework corrects missing and
876   underestimated secondary organic aerosol sources. One Earth [J], 5(403-412.
877 Chang Y, Gao Y, Lu Y, et al. 2021. Discovery of a Potent Source of Gaseous Amines in Urban China.
878   Environmental Science & Technology Letters [J], 8(9): 725-731.
879 Chen F, Dudhia J 2000. Coupling an Advanced Land-Surface/Hydrology Model with the Penn
880   State/NCAR MM5 Modeling System. 129(
881 Cheng Y, Su H, Koop T, et al. 2015. Size dependence of phase transitions in aerosol nanoparticles. Nature
882   Communications [J], 6(1): 5923.
883 Chrit M, Sartelet K, Sciare J, et al. 2018. Modeling organic aerosol concentrations and properties during
884   winter 2014 in the northwestern Mediterranean region. Atmos. Chem. Phys. [J], 18(24): 18079-
885   18100.
886 Chu B, Kerminen V-M, Bianchi F, et al. 2019. Atmospheric new particle formation in China.
887   Atmospheric Chemistry and Physics [J], 19(115-138.
888 Dal Maso M, Kulmala M, Riipinen I, et al. 2005. Formation and growth of fresh atmospheric aerosols:
889   Eight years of aerosol size distribution data from SMEAR II, Hyytiälä, Finland. Boreal
890   Environment Research [J], 10(323-336.
891 Davidovits P, Worsnop D R, Jayne J T, et al. 2004. Mass accommodation coefficient of water vapor on
892   liquid water. Geophysical Research Letters [J], 31(22).
893 Donahue N M, Robinson A L, Stanier C O, et al. 2006. Coupled Partitioning, Dilution, and Chemical
894   Aging of Semivolatile Organics. Environmental Science & Technology [J], 40(8): 2635-2643.
895 Dong C, Matsui H, Spak S, et al. 2019. Impacts of New Particle Formation on Short-term Meteorology
896   and Air Quality as Determined by the NPF-explicit WRF-Chem in the Midwestern United States.
897   Aerosol and Air Quality Research [J], 19(2): 204-220.

898   Dusek U, Frank G P, Hildebrandt L, et al. 2006. Size Matters More Than Cloud-Nucleating
899   Ability of Aerosol Particles. Science [J], 312(5778): 1375-1378.

900   Ehn M, Thornton J, Kleist E, et al. 2014. A large source of low-volatility secondary organic aerosol.
901   Nature [J], 506(476-479.

902   Fanourgakis G S, Kanakidou M, Nenes A, et al. 2019. Evaluation of global simulations of aerosol particle
903   and cloud condensation nuclei number, with implications for cloud droplet formation. Atmos.
904   Chem. Phys. [J], 19(13): 8591-8617.

905   Gordon H, Kirkby J, Baltensperger U, et al. 2017. Causes and importance of new particle formation in
906   the present-day and preindustrial atmospheres. 122(16): 8739-8760.

907   Grell G A 1993. Prognostic Evaluation of Assumptions Used by Cumulus Parameterizations. Monthly
908   Weather Review [J], 121(3): 764-787.

909   Guo S, Hu M, Zamora M L, et al. 2014. Elucidating severe urban haze formation in China. Proceedings
910   of the National Academy of Sciences [J], 111(49): 17373-17378.

911   Hong S-Y, Noh Y, Dudhia J 2006. A New Vertical Diffusion Package with an Explicit Treatment of
912   Entrainment Processes. Monthly Weather Review - MON WEATHER REV [J], 134(

913   Hudson J G, Noble S 2014. CCN and Vertical Velocity Influences on Droplet Concentrations and
914   Supersaturations in Clean and Polluted Stratus Clouds. Journal of the Atmospheric Sciences [J],
915   71(1): 312-331.

916   Iacono M, Delamere J, Mlawer E, et al. 2008. Radiative Forcing by Long-Lived Greenhouse Gases:
917   Calculations with the AER Radiative Transfer Models. Journal of Geophysical Research [J],
918   113(

919   Jimenez J L, Canagaratna M R, Donahue N M, et al. 2009. Evolution of Organic Aerosols in the
920   Atmosphere. Science [J], 326(5959): 1525-1529.

921   Kalkavouras P, Bougiatioti A, Kalivitis N, et al. 2019. Regional new particle formation as modulators of
922   cloud condensation nuclei and cloud droplet number in the eastern Mediterranean. Atmos. Chem.
923   Phys. [J], 19(9): 6185-6203.

924   Kerminen V-M, Chen X, Vakkari V, et al. 2018. Atmospheric new particle formation and growth: Review
925   of field observations. Environmental Research Letters [J], 13(

926   Krechmer J E, Day D A, Ziemann P J, et al. 2017. Direct Measurements of Gas/Particle Partitioning and
927   Mass Accommodation Coefficients in Environmental Chambers. Environ Sci Technol [J],
928   51(20): 11867-11875.

929   Kulmala M, Dada L, Daellenbach K R, et al. 2021. Is reducing new particle formation a plausible solution
930   to mitigate particulate air pollution in Beijing and other Chinese megacities? Faraday
931   Discussions [J], 226(0): 334-347.

932   Kulmala M, L L, Lehtinen K, et al. 2004. Initial steps of aerosol growth. Atmospheric Chemistry and
933   Physics [J], 4(

934   Kulmala M, Petäjä T, Ehn M, et al. 2013. Chemistry of Atmospheric Nucleation: On the Recent Advances
935   on Precursor Characterization and Atmospheric Cluster Composition in Connection with
936   Atmospheric New Particle Formation. Annual review of physical chemistry [J], 65(

937   Kulmala M, Petäjä T, Nieminen T, et al. 2012. Measurement of the nucleation of atmospheric aerosol
938   particles. Nature Protocols [J], 7(9): 1651-1667.

939   Lai S, Hai S, Gao Y, et al. 2022. The striking effect of vertical mixing in the planetary boundary layer on
940   new particle formation in the Yangtze River Delta. Science of The Total Environment [J],
941   829(154607.

Lee S-H, Gordon H, Yu H, et al. 2019. New Particle Formation in the Atmosphere: From Molecular Clusters to Global Climate. Journal of Geophysical Research: Atmospheres [J], 124(

Li K, Zhu Y, Gao H, et al. 2015. A comparative study of cloud condensation nuclei measured between non-heating and heating periods at a suburb site of Qingdao in the North China. Atmospheric Environment [J], 112(40-53.

Li M, Liu H, Geng G, et al. 2017. Anthropogenic emission inventories in China: a review. National Science Review [J], 4(6): 834-866.

Li X, Li Y, Cai R, et al. 2022. Insufficient Condensable Organic Vapors Lead to Slow Growth of New Particles in an Urban Environment. Environmental Science & Technology [J], 56(14): 9936-9946.

Liu H J, Zhao C S, Nekat B, et al. 2014a. Aerosol hygroscopicity derived from size-segregated chemical composition and its parameterization in the North China Plain. Atmos. Chem. Phys. [J], 14(5): 2525-2539.

Liu M, Matsui H 2022. Secondary Organic Aerosol Formation Regulates Cloud Condensation Nuclei in the Global Remote Troposphere. Geophysical Research Letters [J], 49(18): e2022GL100543.

Liu X, Zhu Y, Zheng M, et al. 2014b. Production and growth of new particles during two cruise campaigns in the marginal seas of China. Atmospheric Chemistry and Physics [J], 14(

Liu X H, Zhu Y J, Zheng M, et al. 2014c. Production and growth of new particles during two cruise campaigns in the marginal seas of China. Atmos. Chem. Phys. [J], 14(15): 7941-7951.

Lovejoy E R, Curtius J, Froyd K D 2004. Atmospheric ion-induced nucleation of sulfuric acid and water. Journal of Geophysical Research: Atmospheres [J], 109(D8).

Lu H, Wang G, Guo H 2022. Ambient acidic ultrafine particles in different land-use areas in two representative Chinese cities. Science of The Total Environment [J], 830(154774.

Lu Y, Yan C, Fu Y, et al. 2019. A proxy for atmospheric daytime gaseous sulfuric acid concentration in urban Beijing. Atmos. Chem. Phys. [J], 19(3): 1971-1983.

Lupascu A, Easter R, Zaveri R, et al. 2015. Modeling particle nucleation and growth over northern California during the 2010 CARES campaign. Atmos. Chem. Phys. [J], 15(21): 12283-12313.

Ma N, Zhao C, Tao J, et al. 2016. Variation of CCN activity during new particle formation events in the North China Plain. Atmos. Chem. Phys. [J], 16(13): 8593-8607.

Matsui H, Koike M, Kondo Y, et al. 2011. Impact of new particle formation on the concentrations of aerosols and cloud condensation nuclei around Beijing. Journal of Geophysical Research: Atmospheres [J], 116(D19).

Matsui H, Koike M, Takegawa N, et al. 2013. Spatial and temporal variations of new particle formation in East Asia using an NPF-explicit WRF-chem model: North-south contrast in new particle formation frequency. 118(20): 11,647-611,663.

Merikanto J, Spracklen D V, Mann G W, et al. 2009. Impact of nucleation on global CCN. Atmos. Chem. Phys. [J], 9(21): 8601-8616.

Mikkonen S, Romakkaniemi S, Smith J N, et al. 2011. A statistical proxy for sulphuric acid concentration. Atmos. Chem. Phys. [J], 11(21): 11319-11334.

Morrison H, Thompson G, Tatarskii V 2009. Impact of Cloud Microphysics on the Development of Trailing Stratiform Precipitation in a Simulated Squall Line: Comparison of One and Two-Moment Schemes. Monthly Weather Review - MON WEATHER REV [J], 137(991-1007.

984 ~~Napari I, Noppel M, Vehkamäki H, et al. 2002. Parametrization of ternary nucleation rates for H2SO4-~~
985 ~~NH3-H2O vapors. Journal of Geophysical Research: Atmospheres [J], 107(D19): AAC 6-1-~~
986 ~~AAC 6-6.~~

987 Nieminen T, Kerminen V M, Petäjä T, et al. 2018. Global analysis of continental boundary layer new
988   particle formation based on long-term measurements. Atmos. Chem. Phys. [J], 18(19): 14737-
989   14756.

990 Petäjä T, Mauldin I R L, Kosciuch E, et al. 2009. Sulfuric acid and OH concentrations in a boreal forest
991   site. Atmos. Chem. Phys. [J], 9(19): 7435-7448.

992 Pierce J, Riipinen I, Kulmala M, et al. 2011. Quantification of the volatility of secondary organic
993   compounds in ultrafine particles during nucleation events. Atmospheric Chemistry and Physics
994   Discussions [J], 11(14495-14539.

995 Pöschl U, Canagaratna M, Jayne J T, et al. 1998. Mass Accommodation Coefficient of H2SO4 Vapor on
996   Aqueous Sulfuric Acid Surfaces and Gaseous Diffusion Coefficient of H2SO4 in N2/H2O. The
997   Journal of Physical Chemistry A [J], 102(49): 10082-10089.

998 Qiao X, Yan C, Li X, et al. 2021. Contribution of Atmospheric Oxygenated Organic Compounds to
999   Particle Growth in an Urban Environment. Environmental Science & Technology [J], XXXX(

1000 Ren J, Chen L, Fan T, et al. 2021. The NPF Effect on CCN Number Concentrations: A Review and Re-
1001   Evaluation of Observations From 35 Sites Worldwide. Geophysical Research Letters [J], 48(19):
1002   e2021GL095190.

1003 Riipinen I, Sihto S L, Kulmala M, et al. 2007. Connections between atmospheric sulphuric acid and new
1004   particle formation during QUEST III–IV campaigns in Heidelberg and Hyytiälä. Atmos.
1005   Chem. Phys. [J], 7(8): 1899-1914.

1006 Roldin P, Swietlicki E, Massling A, et al. 2011a. Aerosol ageing in an urban plume – implication for
1007   climate. Atmos. Chem. Phys. [J], 11(12): 5897-5915.

1008 Roldin P, Swietlicki E, Schurgers G, et al. 2011b. Development and evaluation of the aerosol dynamics
1009   and gas phase chemistry model ADCHEM. Atmos. Chem. Phys. [J], 11(12): 5867-5896.

1010 Saha S, Moorthi S, Wu X, et al. 2014. The NCEP Climate Forecast System Version 2. Journal of Climate
1011   [J], 27(6): 2185-2208.

1012 Shen X, Sun J, Zhang X, et al. 2018. Comparison of Submicron Particles at a Rural and an Urban Site in
1013   the North China Plain during the December 2016 Heavy Pollution Episodes. Journal of
1014   Meteorological Research [J], 32(26-37.

1015 Shrivastava M, Fast J, Easter R, et al. 2011. Modeling organic aerosols in a megacity: comparison of
1016   simple and complex representations of the volatility basis set approach. Atmospheric Chemistry
1017   and Physics [J], 11(6639-6662.

1018 Shrivastava M K, Lane T E, Donahue N M, et al. 2008. Effects of gas particle partitioning and aging of
1019   primary emissions on urban and regional organic aerosol concentrations. 113(D18).

1020 Sihto S L, Kulmala M, Kerminen V M, et al. 2006. Atmospheric sulphuric acid and aerosol formation:
1021   implications from atmospheric measurements for nucleation and early growth mechanisms.
1022   Atmos. Chem. Phys. [J], 6(12): 4079-4091.

1023 Sihto S L, Mikkilä J, Vanhanen J, et al. 2011. Seasonal variation of CCN concentrations and aerosol
1024   activation properties in boreal forest. Atmos. Chem. Phys. [J], 11(24): 13269-13285.

1025 Tewari M, Wang W, Dudhia J, et al. 2016. Implementation and verification of the united NOAH land
1026   surface model in the WRF model [M].

Virtanen A, Kannosto J, Kuuluvainen H, et al. 2011. Bounce behavior of freshly nucleated biogenic secondary organic aerosol particles. Atmos. Chem. Phys. [J], 11(16): 8759-8766.

Wang D-W, Guo H, Chan C K 2014. Diffusion Sampler for Measurement of Acidic Ultrafine Particles in the Atmosphere. Aerosol Science and Technology [J], 48(12): 1236-1246.

Wang J, Li M, Li L, et al. 2022. Particle number size distribution and new particle formation in Xiamen, the coastal city of Southeast China in wintertime. Science of The Total Environment [J], 826(154208.

Wang Y, Wang Y, Song X, et al. 2023. The impact of particulate pollution control on aerosol hygroscopicity and CCN activity in North China. Environmental Research Letters [J], 18(074028.

Westervelt D M, Pierce J R, Riipinen I, et al. 2013. Formation and growth of nucleated particles into cloud condensation nuclei: model–measurement comparison. Atmos. Chem. Phys. [J], 13(15): 7645-7663.

Wu H, Li Z, Jiang M, et al. 2021a. Contributions of traffic emissions and new particle formation to the ultrafine particle size distribution in the megacity of Beijing. Atmospheric Environment [J], 262(118652.

Wu L, Ling Z, Shao M, et al. 2021b. Roles of Semivolatile/Intermediate-Volatility Organic Compounds on SOA Formation Over China During a Pollution Episode: Sensitivity Analysis and Implications for Future Studies. Journal of Geophysical Research: Atmospheres [J], 126(8): e2020JD033999.

Wu Z, Hu M, Yue D, et al. 2011. Evolution of particle number size distribution in an urban atmosphere during episodes of heavy pollution and new particle formation. Science China Earth Sciences [J], 54(11): 1772.

Yao L, Garmash O, Bianchi F, et al. 2018. Atmospheric new particle formation from sulfuric acid and amines in a Chinese megacity. Science [J], 361(278-281.

Yu F 2005. Quasi-unary homogeneous nucleation of H2SO4-H2O. The Journal of Chemical Physics [J], 122(7): 074501.

Yu F, Luo G, Nair A A, et al. 2020. Wintertime new particle formation and its contribution to cloud condensation nuclei in the Northeastern United States. Atmos. Chem. Phys. [J], 20(4): 2591-2601.

Yu F, Luo G, Pryor S C, et al. 2015. Spring and summer contrast in new particle formation over nine forest areas in North America. Atmos. Chem. Phys. [J], 15(24): 13993-14003.

Yuan Q, Li W, Zhou S, et al. 2015. Integrated evaluation of aerosols during haze-fog episodes at one regional background site in North China Plain. Atmospheric Research [J], 156(102-110.

Yue D L, Hu M, Zhang R Y, et al. 2011. Potential contribution of new particle formation to cloud condensation nuclei in Beijing. Atmospheric Environment [J], 45(33): 6070-6077.

Zaveri R A, Easter R C, Fast J D, et al. 2008. Model for Simulating Aerosol Interactions and Chemistry (MOSAIC). 113(D13).

Zaveri R A, Easter R C, Peters L K 2005. A computationally efficient Multicomponent Equilibrium Solver for Aerosols (MESA). Journal of Geophysical Research: Atmospheres [J], 110(D24).

Zhang Q, Jimenez J L, Canagaratna M R, et al. 2007. Ubiquity and dominance of oxygenated species in organic aerosols in anthropogenically-influenced Northern Hemisphere midlatitudes. Geophysical Research Letters [J], 34(13).

Zhao B, Shrivastava M, Donahue N M, et al. 2020. High concentration of ultrafine particles in the Amazon free troposphere produced by organic new particle formation. Proceedings of the National Academy of Sciences [J], 117(41): 25344-25351.

Zhao B, Wang S, Donahue N M, et al. 2016. Quantifying the effect of organic aerosol aging and intermediate-volatility emissions on regional-scale aerosol pollution in China. Scientific Reports [J], 6(1): 28815.

Zheng B, Tong D, Li M, et al. 2018. Trends in China's anthropogenic emissions since 2010 as the consequence of clean air actions. Atmos. Chem. Phys. [J], 18(19): 14095-14111.

Zhu Y, Li K, Shen Y, et al. 2019. New particle formation in the marine atmosphere during seven cruise campaigns. Atmos. Chem. Phys. [J], 19(1): 89-113.

Zhu Y, Sabaliauskas K, Liu X, et al. 2014. Comparative analysis of new particle formation events in less and severely polluted urban atmosphere. Atmospheric Environment [J], 98(655-664.

Zhu Y, Shen Y, Li K, et al. 2021. Investigation of Particle Number Concentrations and New Particle Formation With Largely Reduced Air Pollutant Emissions at a Coastal Semi-Urban Site in Northern China. Journal of Geophysical Research: Atmospheres [J], 126(17): e2021JD035419.